Weak Magnetic Fields Sensing Using Soft Ferrite Nanoparticles and MEMS

Sergey E. Lyshevski[1] and Karen S. Martirosyan[2]

[1]Department of Electrical and Microelectronic Engineering
Rochester Institute of Technology, Rochester, NY 14623-5603, USA
sergey.lyshevski@mail.rit.edu

[2]Department of Physics and Astronomy
University of Texas at Brownsville, Brownsville, TX 78520, USA
karen.martirosyan@utb.edu

ABSTRACT

We perform the feasibility analysis of sensing weak magnetic fields by using soft ferrite nanoparticles embedded in molecular complexes, microsystems and microelectromechanical systems (MEMS). The sensing mechanisms are based on the deflection of molecular complexes and induced strain due to the varying magnetic force. The proposed premise can be relevant in analysis of sensing weak magnetic fields in biological systems and living organisms. However, phenomena utilized, device physics and analyses can be fundamentally distinct. The feasibility analysis of proof-of-concept solid-state and hybrid microdevices are reported. The fabrication of various soft ferrites are presented.

Keywords: magnetic field, soft ferrites, nanoparticles, molecular complexes, biological systems

1. INTRODUCTION

Some bacteria, migrating ants, bees, birds, fish, lobsters, salamanders, sea turtles and other living organisms likely exhibit the ability to sense the Earth's magnetic field and use the topographical mapping of the geomagnetic field for navigation, homing, foraging, etc. [1-7]. The magnetic properties of the closely-spaced biomineralized magnetite chains (~50 nm in diameter and length magnetites with ~5 nm separation) are used by magnetotactic bacteria for propulsion. The iron oxide particles and their complexes are found in various living organisms, some of which are illustrated in Figure 1. These facts led to a hypothesis that intracellular biomineralized iron oxides could interact with the geomagnetic field. This can result in sensing direction, variations, intensity and gradient of weak magnetic field by *microscopic* or *macroscopic* biomolecular *fabrics*. The fundamental processes and mechanisms, used by living organisms to detect the geomagnetic field, have being debated and are under extensive studies [1-7].

A great variety of biomineralized iron oxide particles (maghemite γ-Fe_2O_3 and ε-Fe_2O_3, magnetite Fe_3O_4, hematite α-Fe_2O_3 and β-Fe_2O_3, wuestite FeO and other) were found within distinct orientation, patterns, etc. The size, shape, morphology, crystallography, spacing, magnetic moment orientation (single-domain, two-domain, superparamagnetic, etc.), magnetic dipole moment, magnetic and thermal stability, as well as other properties of biomineralized iron oxide particles and clusters vary. The biomineralized magnetic iron oxides and corresponding receptors could constitute magnetoreceptor cellular assemblies within the peripheral and central nervous systems. Theoretically, these magnetoreceptors can sense the weak geomagnetic field utilizing the electrochemo-mechanical transductions or quantum-mechanical *state* transitions.

Figure 1: Fire ant, rainbow trout (*Oncorhynchus mykiss*), sockeye salmon (*Oncorhynchus nerka*) and homing pigeon.

2. FEASIBILITY ANALYSIS

We focus on conventional electromagnetics for *meso-* and *macroscopic* systems for which well-developed technologies (CMOS, micromachining, synthetic chemistry and other) exist. To potentially contribute to the biophysics of *natural* systems and apply the results to *engineered* systems, we study the interactive electromagnetic-mechanical phenomena of clustered magnets (magnetic particles and assemblies) with various molecular (*microscopic*), *mesoscopic* and *macroscipic* (*bulk*) receptors' and sensors' assemblies. It is found that weak magnetic field variations result in sufficient changes in the *mesascopic* system states and quantities. These transitions can be utilized guarantying the overall functionality [8]. The sensing mechanism can be based on the changes of physical quantities (variations of strain, charge, conformation, etc.) caused by the interaction of magnetic

clusters, which have the magnetic dipole moment **m**(**r**), with the field **B**.

3. FABRICATION OF Ni-Zn AND Mn-Zn FERRITES

Ferromagnetic nickel-zinc and manganese-zinc ferrites $Me_xZn_{1-x}Fe_2O_4$ (Me denotes Ni or Mn, 0.1<x<0.9) are widely used in to fabricate components for microwave and communication. Important properties of these ferrites are the initial permeability (100-2000), residual and saturation magnetization (up to 0.2 and 0.4 T) and the coercive field (less than 1 kA/m).

Recently, a novel synthesis approach was developed to synthesize complex oxides, e.g., *Carbon Combustion Synthesis of Oxides* (CCSO) [9-14]. In CCSO the exothermic oxidation of carbon ($C+O_2=CO_2$ $\Delta H^{298}_{CO_2}$=-393.5 kJ/mol) generates a steep thermal reaction wave which propagates at a velocity of 0.1-3 mm/s through the solid reactant mixture (oxides, carbonates or nitrates) converting it to the desired oxide product by the following reaction [9]

$$\sum_{i=1}^{n} \mu_i X_i^{(s)} + \alpha C^{(s)} + \beta O_2^{(g)} = \sum_{j=1}^{m} P_j^{(s)} + \delta CO_2^{(g)} + (-\Delta H)$$

where $\alpha = \dfrac{x/12}{(100-x)/\sum \mu_i M_i^{(s)}}$

We perform the synthesis of the $Ni_{0.35}Zn_{0.65}Fe_2O_4$ and $Mn_{0.25}Zn_{0.75}Fe_2O_4$ ferrites using the reactions:

$$0.35NiO + 0.65ZnO + Fe_2O_3 + \alpha(C + O_2) \Rightarrow Ni_{0.35}Zn_{0.65}Fe_2O_4 + \alpha CO_2\uparrow \quad (1)$$

$$0.25MnCO_3 + 0.75ZnO + Fe_2O_3 + \alpha(C + O_2) \Rightarrow Mn_{0.25}Zn_{0.75}Fe_2O_4 + (\alpha+0.25)CO_2\uparrow, \quad (2)$$

at $2<\alpha<14$.

The temperature in the reaction zone increases at a rate of 70 and 40 °C/s during the synthesis of Ni-Zn and Mn-Zn ferrites, respectively. The maximum combustion temperatures and rate of temperature rise during the synthesis of Ni-Zn ferrite by reaction (1) were higher compare with those of Mn-Zn ferrite by reaction (2) at the same carbon concentration. The lower value was caused by the heat consumed by the decomposition of the manganese carbonate by the reaction $3MnCO_3 \rightarrow Mn_3O_4+CO+2CO_2$.

The synthesized Ni-Zn and Mn-Zn ferrites powders produced at different carbon concentrations have soft magnetic properties [10-12]. A higher carbon concentration increases the saturation magnetization B_{max}, decreases the remanent magnetization B_r, and, dicreass the coercitive field H_c. Increasing the carbon concentration in the reactant mixture increases the reaction temperature and consequently the product grain size. The ac conductivity of the as-synthesized Ni-Zn ferrites increases with increasing applied frequency and carbon concentration in the mixture as illustrated in Figure 2.

The powders have low ac conductivity σ, and, σ varies from ~1×10^{-4} to 1×10^{-5} S/m at 20 MHz. These properties are needed in high frequency applications. The Ni-Zn and Mn-Zn ferrites, prepared using the CCSO process, have soft-magnetic properties such as:

H_c=46-95 A/m, B_r=0.11-0.18 T, B_{max}=0.28-0.32 T and μ_r=340-520.

Therefore, the fabricated ferrites have favorable characteristics comparable with ferrites produced by the other methods.

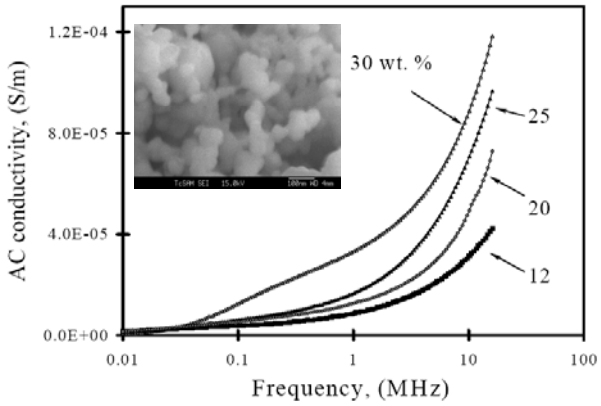

Figure 2: AC-conductivity of Ni-Zn ferrites (sintered at the temperature 1150 °C) as a function of frequency, measured at the room temperature. Inset immage: A typical microstructure of synthesized ferrites.

The magnetic properties of the sintered Ni-Zn ferrites at three different temperatures of 1050 °C, 1150 °C and 1250 °C were determined from their hysteresis loops. The results are presented in Table 1. After sintering of Ni-Zn ferrites at 1250 °C, the sample density of 5.0 g/cm^3, is 96 % of the theoretical value.

Table 1. Magnetic properties and bulk density of sintered Ni0.35Zn0.65Fe2O4 samples at different temperatures.

Properties	Sintering temperature, (°C)		
	1050	1150	1250
B_{max}, (T)	0.28	0.30	0.32
B_r(T)	0.18	0.14	0.11
H_c (A/m)	95	62	46
σ, S/m (10 MHz)	2.8×10^{-5}	3.5×10^{-5}	4.6×10^{-5}
μ, (100 kHz)	340	540	620
Bulk density, (g/cm^3)	4.83	4.94	5.0

The sintering of as-synthesized powder shows that increasing the annealing temperature from 1050 to 1250 °C considerably increased the saturation magnetization and

reduced the value of H_c and B_r. The optimal magnetic properties were obtained by annealing at a temperature of 1150 °C. The magnetic properties of the sintered samples (Table 1) compare well with the commercial ferrites produced by others methods. These ferrites is employed to fabricate MEMs devices having components for weak magnetic field sensing.

4. ELECTROMAGNETICS WITH APPLICATIONS

In the pigeon beak, the ~3 nm magnetites are arranged in organized ~1 μm diameter ferromagnetic or superparamagnetic clusters (assembly of ferrimagnetic or ferromagnetic particles in non-ferromagnetic matrix) within dendrites. In addition, the maghemite clusters occur around the vesicle (diameter ~5 μm) as well as ~10 μm-long bundles of single crystalline uniform square platelets (~1×1×0.1 μm) within the dendrite in the ordered pattern. A ferromagnetic magnetite (the orbital and spin magnetic dipole moments obey $|m_{spin}|>|m_{orb}|$) exhibits a response to an external magnetic field. We consider:

1. Electromagnetic interactions of *macroscopic* ferromagnetic and superparamagnetic particles/clusters which lead to electromagnetic-mechanically induced transductions in biomolecular assemblies. Single-domain magnetite has been localized in the nervous system of various living organisms, and, correspondingly, may result in the subcellular level of sensory, memory and processing;
2. Microfluidics. The ordered, disordered and controlled dynamic and static behavior of particles (typical size is from ~10 nm to ~10 μm) can result in the electro-magnetic field-induced viscoelastic, strain-caused and other transductions. The behavior of magnetite clusters can be used in *engineered* systems. There are issues associated with the fact that the arrangement and morphology of the magnetite in the dendrites, receptors and subcellular structures may not be accuratly analyzed. These problems are overcome in the *macroscopic engineered* devices.

One recalls that

$$\mathbf{B}=\mu_0(\mathbf{H}+\mathbf{M}),\ \mathbf{M}=\chi_m\mathbf{H},\ \mathbf{B}=\mu_0\mu_r\mathbf{H},$$

where χ_m is the magnetic susceptibility; μ_r is the relative permeability, $\mu_r=1+\chi_m$.

For FeO, the magnetic molar susceptibility $\chi_m V_m$ is 7.2×10^9 cm^3/mol, where V_m is the molar volume.

For the organic compounds (C_2H_2, C_6H_6, $C_6H_{12}O_2$, $C_{20}H_{12}$, etc.), the diamagnetic molar susceptibility varies from $\sim2.5\times10^7$ to 20×10^7 cm^3/mol.

Consider the translational and *torsional-mechanical* motion of magnetic clusters in the magnetic field. The electromagnetic translational and rotational motions result due to the force and torque developed. The torque **T** tends to align **m** with **B**, and

$$\mathbf{T}=\mathbf{m}\times\mathbf{B}.$$

For a magnetic rod with the length l and the pole strength Q_m, the magnetic moment is

$$m=Q_m l,$$

while the force is

$$F=Q_m B.$$

The electromagnetic torque is given as

$$T=2F½l\sin\alpha=Q_m lB\sin\alpha=mB\sin\alpha.$$

Thus,

$$\mathbf{T}=\mathbf{a}_m m\times\mathbf{B}=Q_m l\mathbf{a}_m\times\mathbf{B},$$

where $\mathbf{a}_m$ is the unit vector in the magnetic moment direction.

With the average magnetic field of the Earth ~50 μT, which varies ~±0.5 μT, the torque is estimated to be ~1 pN-m. The Newtonian translational and *torsional-mechanical* dynamics are governed by the differential equations

$$\Sigma\mathbf{F}=m_m\boldsymbol{a}\ \text{and}\ \Sigma\mathbf{T}=J\boldsymbol{\alpha}.$$

where $\boldsymbol{a}$ and $\boldsymbol{\alpha}$ are the linear and angular accelerations,

$$\boldsymbol{a}=d\mathbf{v}/dt=d^2\mathbf{r}/dt^2,\ \boldsymbol{\alpha}=d\boldsymbol{\omega}/dt=d^2\mathbf{r}/dt^2;$$

m_m and J are the mass and moment of inertia.

Using the pole strength Q_m, the force acting on a magnet is

$$\mathbf{F}=\mathbf{B}Q_m.$$

The force between two magnets depends on the shape, magnetization, orientation, etc. The Coulomb law provides the equation for the force. For two magnetic poles we have

$$\mathbf{F}=\mathbf{a}_r\frac{\mu_0}{4\pi}\frac{Q_{m1}Q_{m2}}{r^2},$$

where $\mathbf{a}_r$ is the unit vector along line joining poles; Q_{m1} and Q_{m2} are the pole strengths; r is the distance between poles.

The flux density at distance r from a pole with Q_m is

$$\mathbf{B}=\mathbf{a}_r\frac{\mu_0}{4\pi}\frac{Q_m}{r^2}.$$

The quantitative analysis is performed to study the magneto-receptor-centric and *engineered* magnetic field sensing.

5. ENGINEERED MAGNETIC FIELD SENSORS

Polymer microcapsules with embedded magnetic particles can be synthesized. The polymer microcapsule's shells are formed as magnetic particles, dispersed in the hydrophobic polymer (for example, NOA prepolymer), are captured into the solid polymer phase at the emulsification step with the subsequent curing and drying. These oxides and microcapsules can be deposited on the movable diaphragm. The magnetic field can be sensed and measured as the membrane deflection. The membrane deflects, one may measure the capacance difference ΔC or induced *emf*. We recall that for a parallel-plate capacitor,

$$\Delta C=\varepsilon A/d$$

while $emf=\oint_l\mathbf{E}\cdot d\mathbf{l}=\oint_l(\mathbf{v}\times\mathbf{B})\cdot d\mathbf{l}-\oint_s\frac{\partial\mathbf{B}}{\partial t}d\mathbf{s}$.

Hence, the time- and spatially-varying displacement results in ΔC or *motional emf*. One can sense the variations of ΔC and *emf* using ICs. These ICs can be integrated

within MEMS technology to fabricate microsystems.

The micromachined structures, components, proof-of-concept devices and prototypes were designed and fabricated as reported in Figure 3.a [8]. The deflection of the suspended (released) movable structures or diaphragms can be measured by using the variations of capacitance and resistance. The micromachined four polysilicon resistors, which form the Wheatstone bridge, are documented in Figure 3.a [8].

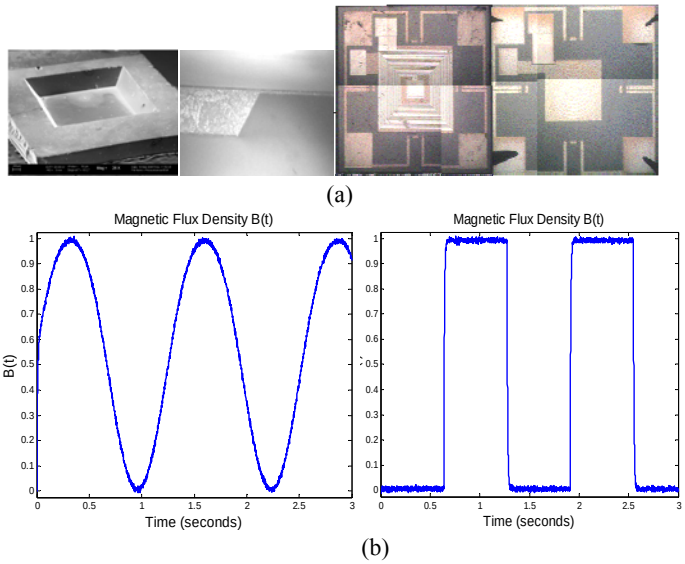

Figure 3: (a) Etched silicon structure, ~30 μm silicon diaphragm, and micromachined sensors with polysilicon resistors (to measure the force-induced membrane deflections) and Al coils on the silicon diaphragm; (b) Sensing time-varying magnetic field $B(t)$.

The magnetic field is measured by using the force-induced displacement-centric sensing mechanism. Figure 3.b documents the deflection of the suspended diaphragm measuring

$B(t)=½[\sin(¼\pi t)-1]$ and $B(t)=½[\mathrm{rect}(¼\pi t)-1]$ mT.

The noise $\xi(t)$ can be filtered by notch or other ilters which can be implemented using ICs. We conclude that it is possible to accurately sense time-varying **B**. These sensors can be used in high-perromance navigation systems.

6. CONCLUSIONS

The fabrication method of soft ferrites $Ni_{0.35}Zn_{0.65}Fe_2O_4$ and $Mn_{0.25}Zn_{0.75}Fe_2O_4$ for weak magnetic filed sensing are presented. The quantitative analysis is performed to study the magneto-receptor-centric and engineered magnetic field sensing by using MEMs devices.

ACKNOWLEDGMENTS

Dr. Martirosyan acknowledges the financial support of this research by the National Science Foundation, grant # 0933140.

REFERENCES

[1] T. Alerstam, *Bird Migration*, Cambridge University Press, Cambridge, 1990.

[2] Y. Camlitepe and D. J. Stradling, "Wood ants orient to magnetic fields," *Proc. R. Soc. Lond.* B, vol. 261, pp. 37-41, 1995.

[3] J.L. Gould, "The case for magnetic sensitivity in birds and bees (such as it is)," *Am. Sci.*, vol. 68, pp. 256-267, 1980.

[4] J.L. Kirschvink, M. M. Walker, and C. E. Diebel, "Magnetite-based magnetoreception," *Current Opinion in Neurobiology*, vol. 11, pp. 462-467, 2001.

[5] C. Walcott, "Magnetic orientation in homing pigeons," *IEEE Trans. Magnet. Mag.*, vol. 16, pp. 1008-1013, 1980.

[6] R. Wiltschko and W. Wiltschko, *Magnetic Orientation in Animals*, Heidelberg: Springer-Verlag, Berlin, 1995.

[7] S. Johnsen and K. J. Lohmann, "The physics and neurobiology of magnetoreception," *Nature*, vol. 6, pp. 703-712, 2005.

[8] I. Puchades, R. Pearson, L. F. Fuller, S. Gottermeier and S. E. Lyshevski, "Design and fabrication of microactuators and sensors for MEMS," *Proc. IEEE Conf. Prospective Technologies and Methods in MEMS Design*, Polyana, Ukraine, pp. 38-44, 2007.

[9] K. S. Martirosyan and D. Luss, Carbon combustion synthesis of oxides, US Patent # 7897135, 2011.

[10] K. S. Martirosyan and D. Luss, Carbon combustion synthesis of ferrites: synthesis and characterization, *Ind. Eng. Chem. Res*., 46, p.1492-1499, 2007.

[11]K. S.Martirosyan, M.Iliev and D.Luss, "Carbon combustion synthesis of nanostructured perovskites, *Int. J. SHS*, 16, p.36-45, 2007.

[12]K. S. Martirosyan, L. Chang, J. Rantschler, S. Khizroev, D. Luss and D. Litvinov, Carbon combustion synthesis and magnetic properties of cobalt ferrite nanoparticles, *IEEE Transactions on Magnetics*, 43, 6, p.3118-3120, 2007.

[13] K. S. Martirosyan, Carbon Combustion Synthesis of Ceramic Oxides Nanopowders, Advances in Science and Technology, 63, 236-245, 2010.

[14] K. S. Martirosyan, E. Galstyan, S. M. Hossain, Yi-Ju Wang and D. Litvinov, Barium hexaferrite nanoparticles: synthesis and magnetic properties, Materials Science & Engineering B, 176, 8-13, 2011.